Computers and Structures 87 (2009) 651–663

Contents lists available at ScienceDirect

Computers and Structures

journal homepage: www.elsevier.com/locate/compstruc

Numerical study of interference between simple-shape bodies in hypersonic flows

Vladimir V. Riabov *

Department of Mathematics and Computer Science, Rivier College, Nashua, NH 03060, United States

ARTICLE INFO

Article history:
Received 20 May 2008
Accepted 24 October 2008
Available online 3 December 2008

Keywords:
Hypersonic rarefied-gas flows
Direct simulation Monte-Carlo method
Flow interference
Simple-shape bodies
Toroidal balloon

ABSTRACT

Hypersonic rarefied-gas flows near two side-by-side plates and cylinders, toroidal balloon, plate and cylinder over a plane surface, and plate behind a cylinder in argon, nitrogen, oxygen, and carbon dioxide have been studied numerically using the direct simulation Monte-Carlo technique under the transition flow conditions at Knudsen numbers from 0.004 to 10. Strong influences of the geometrical factor (the ratio of a distance between bodies to a body length) and the Knudsen number on the flow structure about the bodies (shock-wave shapes, the configuration of subsonic flow zones), skin friction, pressure distribution, lift, and drag have been found.

1. Introduction

Experimental and numerical studies [1–4] of aerodynamics of simple-shape bodies have provided valuable information related to physics of hypersonic flows about spacecraft elements and testing devices. Numerous results had been found in the cases of plates, wedges, cones, disks, spheres, torus, and cylinders (see Refs. [1–7]). The interference effect for flat strips and cylinder grids was experimentally studied by Coudeville et al. [8] for transition rarefied-gas flows. Supersonic, subsonic, and pressure-driven, low-speed flows in two-dimensional microchannels of varying aspect ratios, $20 \geqslant L/2H \geqslant 2.5$, were studied with the DSMC technique by Mavriplis et al. [9] and Oh et al. [10] for a range of continuum to transitional rarefied-gas flow regimes. The results [9,10] were in qualitative agreement with other computational and experimental results for longer microchannels. Near the continuum limit, they show the same trends as classical theories, such as Fanno–Rayleigh flow and boundary–layer interaction with shocks [9].

In the present study, the hypersonic rarefied-gas flow about two side-by-side plates of varying small aspect ratios, $2 \geqslant L/2H \geqslant 0.4$, has been studied at Knudsen numbers $Kn_{\infty,L}$ from 0.024 to 1.8. The flow pattern for such a configuration has not been discussed in the research literature. Numerical results have been obtained using the direct simulation Monte-Carlo (DSMC) technique [2] and the computer code [11] developed by Graeme Bird. Several features of the flow are unique. For example, if the distance between the plates, $2H$, is significantly larger than the plate length L, then the flow can be approximated by a stream between two isolated plates [2–6]. At $H \leqslant 0.25L$, the rarefied-gas flow has some features of a stream near a bluff body [12]. In the first case, two oblique shock waves interact in the vicinity of the symmetry plane generating the normal shock wave and the Mach reflected waves far behind the bodies. In the second case, the front shock wave would be normal and the pressure and skin-friction distributions along the upper and bottom surfaces would be difficult to predict. At $H \leqslant 0.5L$, the flow pattern and shock-wave shapes are very complex. Therefore, simple approximations should not be used to define the aerodynamics of side-by-side bodies.

Flow about two side-by-side cylinders, their aerodynamic characteristics, and interference between cylinder and a plane surface have also been studied under the conditions of a hypersonic rarefied-gas stream at Knudsen numbers $Kn_{\infty,R}$ from 0.0167 to 10 and a range of geometrical factors ($6R \geqslant H \geqslant 2R$). For $3R \geqslant H$, the repulsive lift force has been found to become significant with a lift-drag ratio of 0.35. Blevins [12] previously analyzed the continuum streams.

Finally, the rarefied-nitrogen flow about a blunt plate located in the wake of a cylindrical wire has been numerically studied. Hayes and Probstein [13], Oguchi [14], and Allègre and Bisch [15] showed that the skin friction and pressure coefficients are maximal near the leading edge of the plate. Bisch [16] offered a unique experimental technique of the friction reduction by adding a wire-shaped "fore-leading edge" in front of the plate. The identical study of continuum flow regimes was made by Yegorov et al. [17]. It was found that the induced wake flow in front of the plate reduced the strength of the shock wave and resulted in reducing the plate drag and friction.

* Tel.: +1 603 897 8613; fax: +1 603 897 8805.
E-mail address: vriabov@rivier.edu

0045-7949/$ - see front matter © 2008 Elsevier Ltd. All rights reserved.
doi:10.1016/j.compstruc.2008.10.010

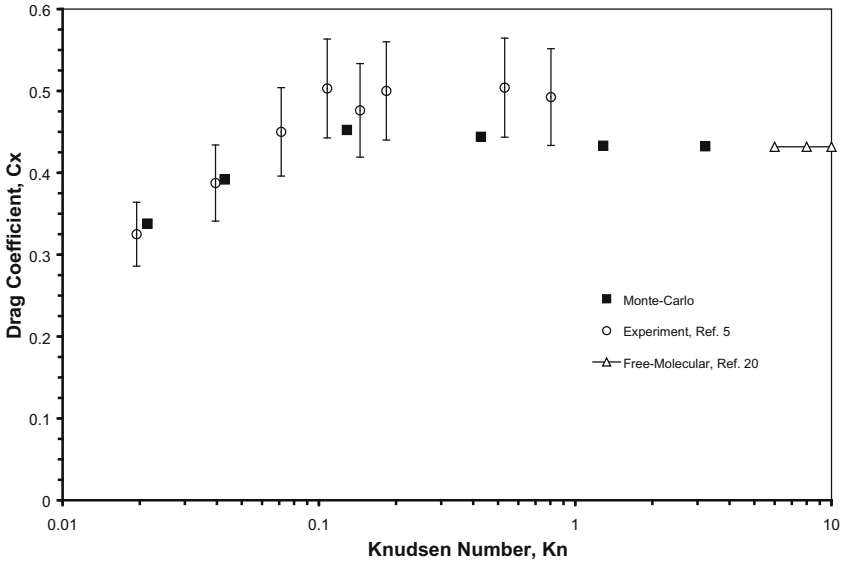

Fig. 1. Total drag coefficient of the plate vs. Knudsen number $Kn_{\infty,L}$ in air at $M_\infty = 10$.

2. DSMC method

The direct simulation Monte-Carlo (DSMC) method (described in detail in Bird's book [2]) and the two-dimensional DS2G code [11] have been used in this study as a numerical simulation technique for low-density hypersonic gas flows. The DSMC method is a computer-simulating technique for the modeling of real-gas effects by a sample of randomly-selected molecules (thousands or even millions). The position coordinates and velocity components of these molecules are stored in the computer memory and are modified with time as the molecules are concurrently followed through representative collisions and boundary interactions in the simulated physical space [2,11].

Table 1
Drag coefficient of a single plate in airflow at $Kn_{\infty,L} = 0.13$, $M_\infty = 10$, $\gamma = 1.4$, $t_w = 1$, and different numerical parameters.

Number of cells	Number of molecules per cell	Drag coefficient	Time of calculation
12,700	11	0.4524	12 h 28 min
12,700	22	0.4523	21 h 03 min
49,400	11	0.4525	62 h 06 min
203,200	11	0.4526	187 h 11 min

Intermolecular collisions in dilute gases are overwhelmingly likely to be binary collisions involving just two molecules. Given the physical properties of the molecules and the orientation of the trajectories, the post-collision velocities are determined from the equations of linear momentum and energy that must be conserved in the collision (see [2, pp. 30–41] for detail).

This direct simulation of the physical processes [2] contrasts with the "traditional" approach of computational fluid dynamics

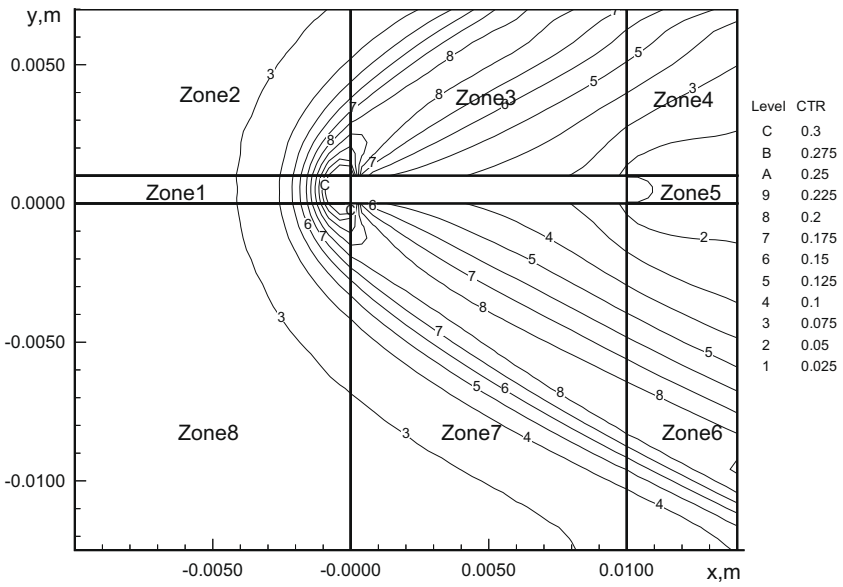

Fig. 2. CTR [11] of the time step to the local mean collision time in argon flow about a side-by-side plate at $Kn_{\infty,L} = 0.024$ and $H = 1.25L$.

(CFD), which is based on obtaining numerical solutions of the fundamental mathematical equations and proper boundary conditions that model the processes [17]. In the cases of rarefied-gas flows, when the gas density is sufficiently low, the direct physical simulation becomes a valuable simulating approach without any recourse to the conventional mathematical models of the flow. Under these conditions, the DSMC method becomes a unique adequate tool, because the full set of the Navier–Stokes equations [3,17,23] (or their modifications, e.g., thin-viscous-shock-layer equations [29]) does not provide a valid model for rarefied gases, and conventional CFD methods are unable to handle the large number of independent variables that are involved in applications of the Boltzmann equation [2,30] to realistic multi-dimensional problems [2]. It has been shown [32] that the Boltzmann equation can be derived though physical reasoning, which is very close to that behind the DSMC procedures, and the two are entirely consistent. For example, the assumptions of molecular chaos and a dilute gas are required by both the Boltzmann formulation and the DSMC method. The major difference between them is the DSMC method does not depend on the existence of inverse collisions [2,32].

The Knudsen number, which is the ratio of the mean free path to a typical dimension of the flowfield (e.g., a cylinder diameter, a plate length, etc.), characterizes the degree of rarefaction of a gas flow. The Navier–Stokes equations [17] are valid when the Knudsen number is very small in comparison with unity [2,3]. The opposite limit (as the Knudsen number tends to infinity) is

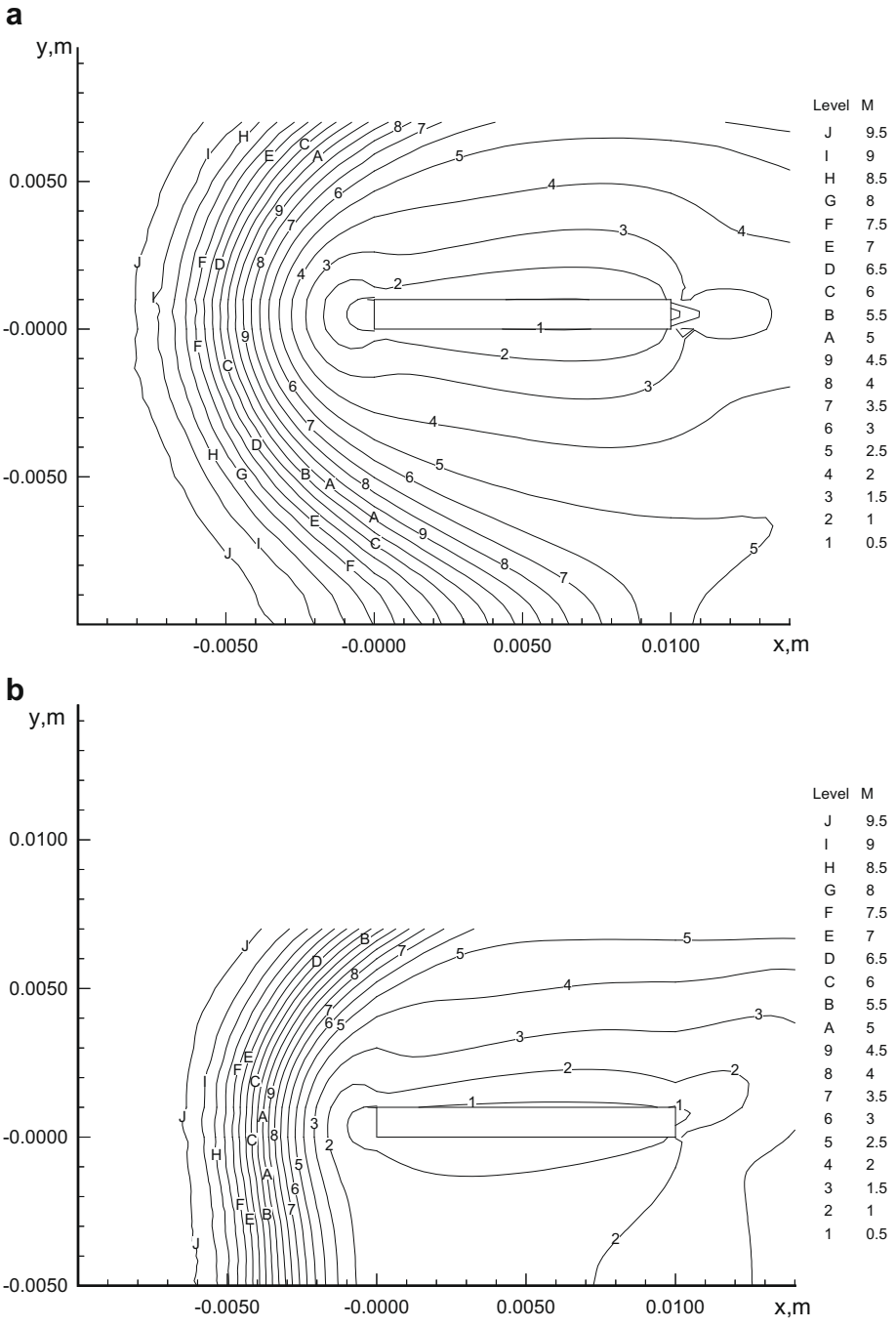

Fig. 3. Mach number contours in argon flow about a side-by-side plate at $Kn_{\infty,L} = 0.024$ and various H/L-ratios: (a) $H = L$ and (b) $H = 0.5L$.

the collisionless or free-molecule flow limit [20], in which intermolecular collisions may be neglected. The flow regime between free-molecule and the limit of validity of the Navier–Stokes equations is generally referred to as the transition flow regime (studied in this paper). A Knudsen number of 0.1 has traditionally been quoted as the boundary between the continuum and transition regimes [2], but the characteristic dimension of complex flow fields may be specified in many different ways and the use of an "overall Knudsen number" may be misleading [11].

The conservation equations of gas dynamics are valid for all flow regimes, but the Navier–Stokes equations depend also on postulates of the Chapman–Enskog theory [30] for the shear stresses,

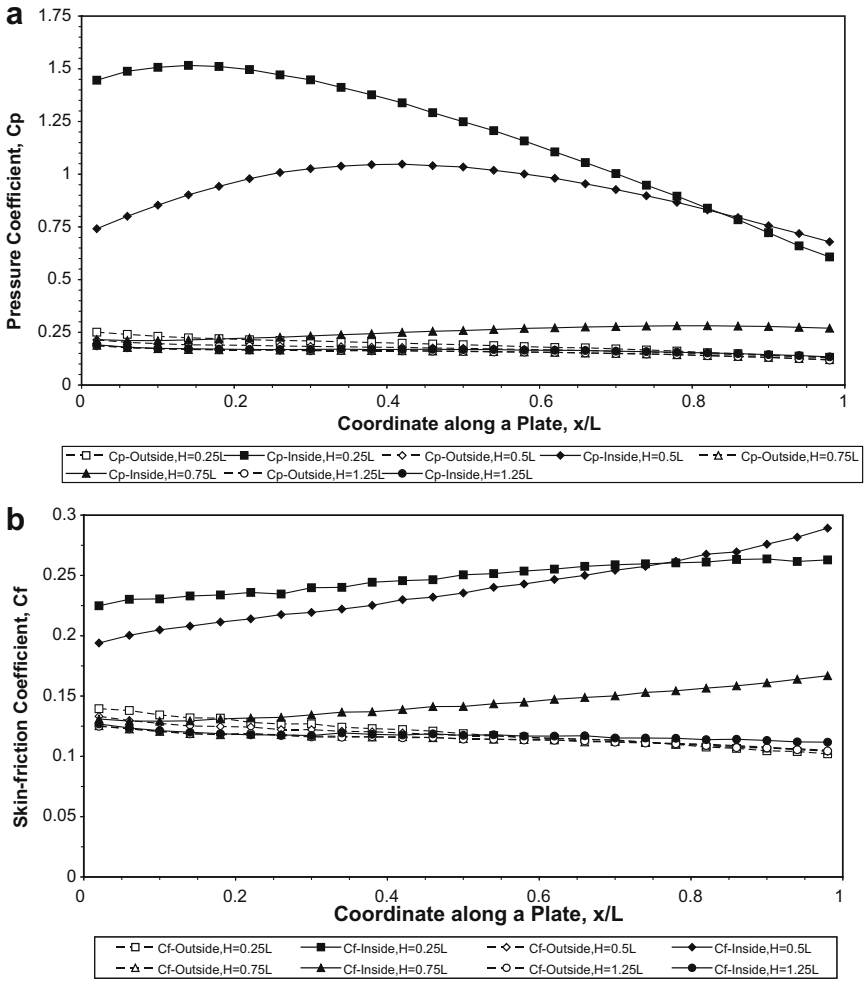

Fig. 4. Pressure and skin-friction coefficients along the side-by-side plate at $Kn_{\infty,L} = 0.024$ at $M_\infty = 10$: (a) pressure coefficient and (b) skin-friction coefficient.

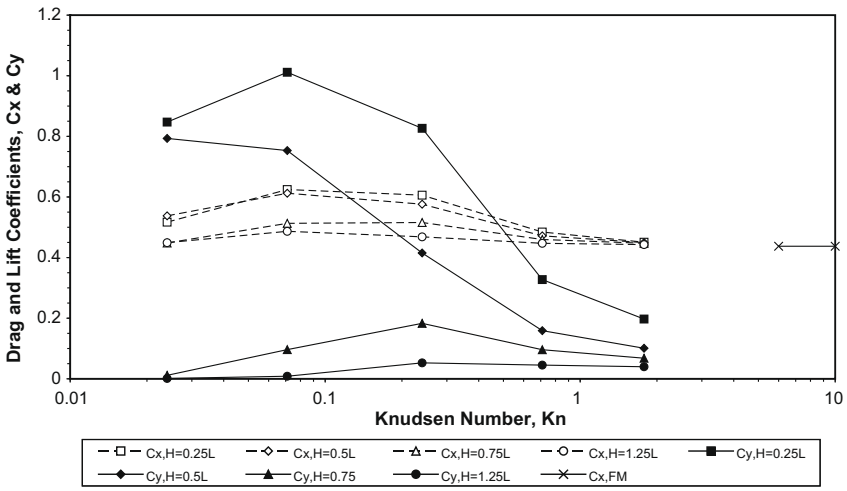

Fig. 5. Total drag and lift coefficients of the side-by-side plates vs. Knudsen number $Kn_{\infty,L}$ at $M_\infty = 10$.

heat fluxes and diffusion velocities as linear functions of the velocity, temperature and concentration gradients. The Chapman–Enskog theory assumes that the velocity distribution is a small perturbation of the equilibrium (or Maxwellian) distribution. The formulation of the Chapman–Enskog distribution incorporates "local Knudsen numbers" [2,30] which are the ratios of the local mean free paths to the scale lengths of the velocity and temperature gradients. It has been found that errors become significant when these local Knudsen numbers exceed 0.1 and the continuum theory is hardly useable when they exceed 0.2 [2]. Although it was shown many years ago [2,30] that the Chapman–Enskog expansion for the distribution function is not uniformly valid, attempts are still being made to extend the range of validity of the Navier–Stokes equations to lower densities (e.g., see [3]).

In addition, some physical effects, such as thermal and pressure diffusion, become more prominent at low densities and these are not generally included in the Navier–Stokes formulations [2]. Once the density becomes sufficiently low, the application of the DSMC method becomes computationally more feasible for the following reasons [11]:

- The calculation is always unsteady with physical time as one of the principal variables in the simulation. A steady flow is obtained as the large time state of the unsteady flow. The method does not require an initial approximation to the flow field and there is no iterative procedure for convergence to the final solution. (In the case of a time averaged steady flow or an ensemble averaged unsteady flow, there will be a gradual decline in the statistical scatter as the sample increases [2]).
- Additional effects, such as non-equilibrium chemistry (e.g., see Section 7), may be included simply by adding to the complexity of the molecular model [2,28] and the fact that these may change the basic nature of the continuum equations is of no consequence.
- Finally (and importantly), there are no numerical instabilities.

Another key computational assumptions associated with the DSMC method are the uncoupling of the molecular motion and collisions over small time steps and the division of the flow field into small cells [2,11]. The time step should be much less than the mean collision time and a typical cell dimension should be much less than the local mean free path [4,11,24]. The cell dimension should also be small compared with the distance over which there is a significant change in the flow properties. In practice, the cell size in low Knudsen number flows is set to about one-third or one-half the cell size [11]. The time step is then set such that a typical molecule moves about one-third of the cell dimension at each time step [2]. This satisfies the above requirement for the size of time step in stationary low Knudsen number flows (considered in this paper).

The DSMC method uses the cell system only for the sampling of the macroscopic properties and for the selection of possible collision partners. In addition, the sampled density is used in the procedures for establishing the collision rate [2]. This means that the cell geometry should be chosen to minimize the changes in the macroscopic properties across an individual cell (as in the code validation case considered in Section 3). Different implementations of the DSMC method (e.g., alternatives in selecting the collision partners in the cells) were discussed in detail in Refs. [2,11]. The latest version 3 of DS2G Program [11], that implements the DSMC method, introduces an adaptive transient rectangular background grid to one cell at a time within the collision routine. This yields nearest-neighbor collisions and is efficient with regard to both computer memory-storage and computation time requirements. The ratio of the time step to the local mean collision time and the ratio of the mean separation between collision partners to the local mean free path should be well under unity over the whole flowfield area.

The replacement of the extremely large number of real molecules by a significantly smaller number of simulated molecules could result (in a few specific cases) in misinterpretation of some physical phenomena. For example, the serious statistical problem arises when a significant effect in the real gas (e.g., chemical reactions of ionization [24], or quantum effects in rotational–translational relaxation in hypersonic under expanded jets [31]) is a consequence of the few molecules towards the extremities of the distribution. In general, the statistical scatter decreases as the square root of the sample size and, in order to attain a sufficiently small standard deviation, the programs employ either time averaging for steady flows [4] or ensemble averaging for unsteady flows [11].

3. Computer code validation

The two-dimensional DS2G code [11] has been used as a numerical simulation tool in this study. Molecular collisions in argon and nitrogen are modeled using the variable hard sphere molecular model [2]. The gas–surface interactions are assumed to

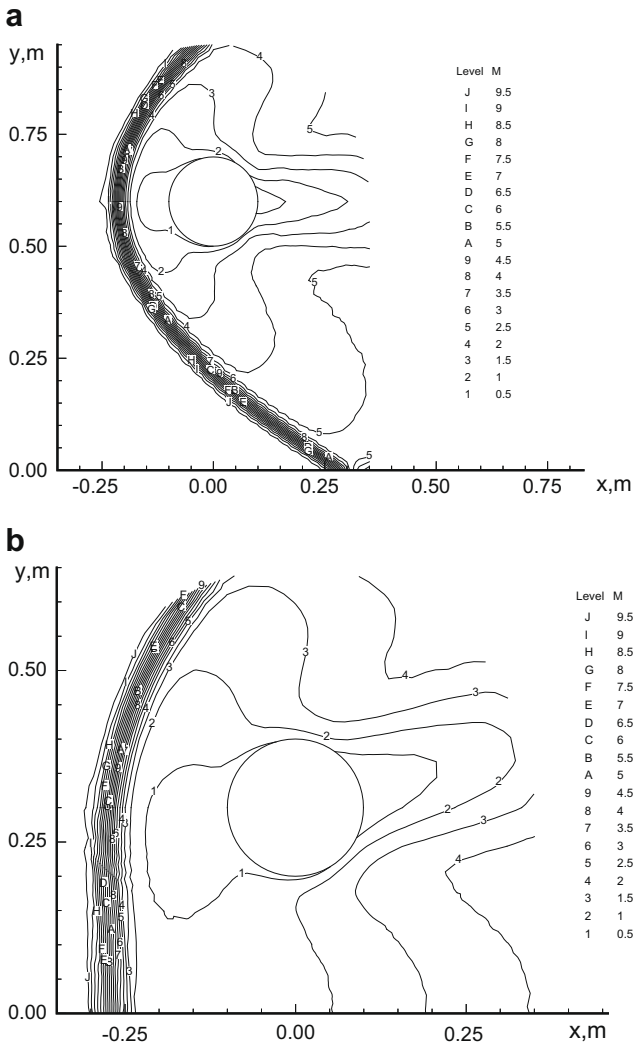

Fig. 6. Mach number contours in argon flow about a side-by-side cylinder at $Kn_{\infty,R} = 0.1$ and various H/R-ratios: (a) $H = 6R$ and (b) $H = 2R$.

be fully diffusive with full moment and energy accommodation, and the wall temperature is equal to the stagnation temperature.

Code validation was established [4,18] by comparing numerical results with experimental data [3,4] related to simple-shape bodies.

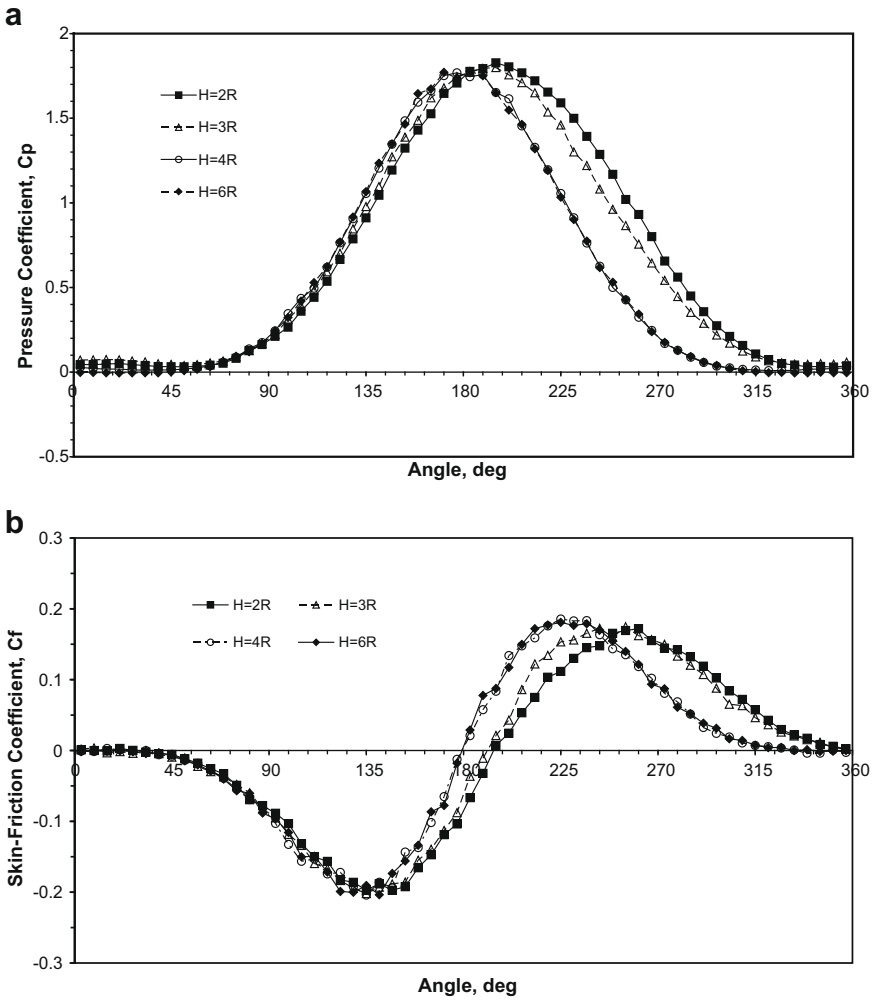

Fig. 7. Pressure and skin-friction coefficients along the side-by-side cylinder at $Kn_{\infty,R} = 0.1$: (a) pressure coefficient and (b) skin-friction coefficient.

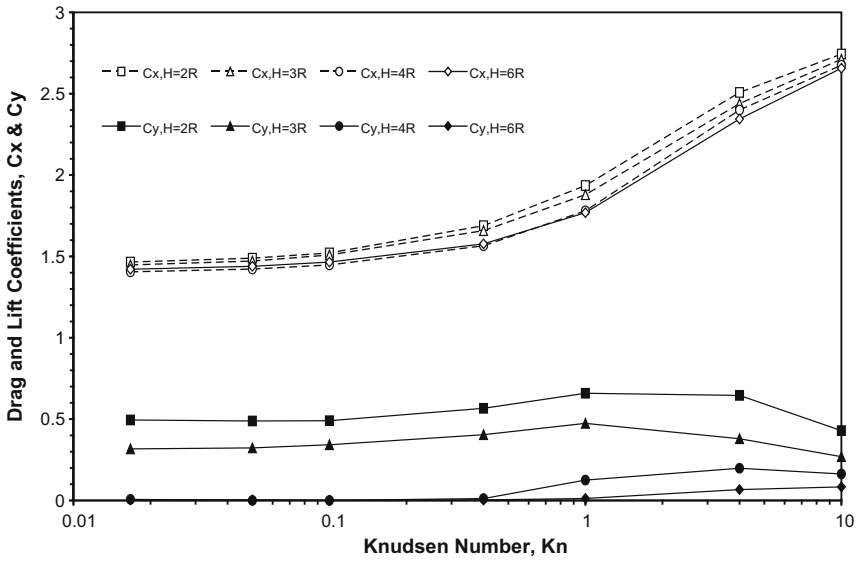

Fig. 8. Total drag and lift coefficients of the side-by-side cylinder vs. Knudsen number $Kn_{\infty,R}$ at $M_\infty = 10$.

As an example, the comparison of the DSMC recent numerical results with experimental data [5] in air is shown in Fig. 1 for a wide range of Knudsen numbers from 0.02 to 3.2 and flow parameters: $M_\infty = 10$, $\gamma = 1.4$, and $t_w = 1$. The error of experimental data [5] (see error bars in Fig. 1) was estimated as 8–12% at different flow regimes (see Ref. [5] and the bibliography in Ref. [4]). The numerical results correlate well with experimental data at $0.02 < Kn_{\infty,L} < 1$ and approach the free-molecular limit [20] at $Kn_{\infty,L} > 3$.

The methodology from Refs. [2,9,11] has been applied in computations. The cases that had been considered by Mavriplis et al. [9] for airflows in near-continuum, transitional and near-free-molecular regimes were reproduced in this study.

The mesh size and the number of molecules per cell were varied until independence of the flow profiles and aerodynamic characteristics from these parameters was achieved for each case [18]. The mesh size and the number of molecules per cell were varied until independence of the flow profiles and aerodynamic characteristics from these parameters was achieved for each case. Table 1 shows the DSMC results for the drag coefficient of the plate C_x in the airflow at $Kn_{\infty,L} = 0.13$, $M_\infty = 10$, $\gamma = 1.4$, $t_w = 1$, and different computational parameters. The uniform grid has covered the symmetrical flow area 0.024 m × 0.021 m near the plate 0.01 m × 0.001 m. The location of the external boundary with the upstream flow conditions is at 0.01 m from the leading edge of the plate. It has been found that the numerical solutions for C_x are independent of the numerical parameters (see Table 1).

The similar mesh parameters have been used in the case of two side-by-side plates. As an example, for calculations at $H/L = 1.25$, the total number of cells near a plate (a half-space of the flow segment between side-by-side plates) is 12,700 in eight zones (see Fig. 2), the argon molecules are distributed evenly, and a total number of 139,720 molecules corresponds to an average 11 molecules per cell. The location of the external boundary with the upstream flow conditions varies from $0.75L$ to $1.5L$. Following the recommendations of Refs. [2,11], acceptable results are obtained for an average of at least 10 molecules per cell in the most critical region of the flow. The error was pronounced when this number falls below five. The cell geometry has been chosen to minimize the changes in the macroscopic properties (pressure and density) across the individual cell [11]. In all cases the usual criterion [2] for the time step Δt_m has been realized, $1 \times 10^{-8} \leqslant \Delta t_m \leqslant 1 \times 10^{-6}$ s. Under these conditions, aerodynamic coefficients and gas-dynamic parameters have become insensitive to the time step. The ratios of the mean separation between collision partners to the local mean free path and the collision time ratio (CTR) [11] of the time step to the local mean collision time have been well under unity over the flowfield (see Fig. 2).

The total number of non-uniform cells [19] near a cylinder (a half-space of the flow segment between side-by-side plates for calculations at $H/R = 3$) is 2100, and 32,200 molecules are distributed evenly (an average 15 molecules per cell). The location of the external boundary varies from $2.5R$ to $4.5R$.

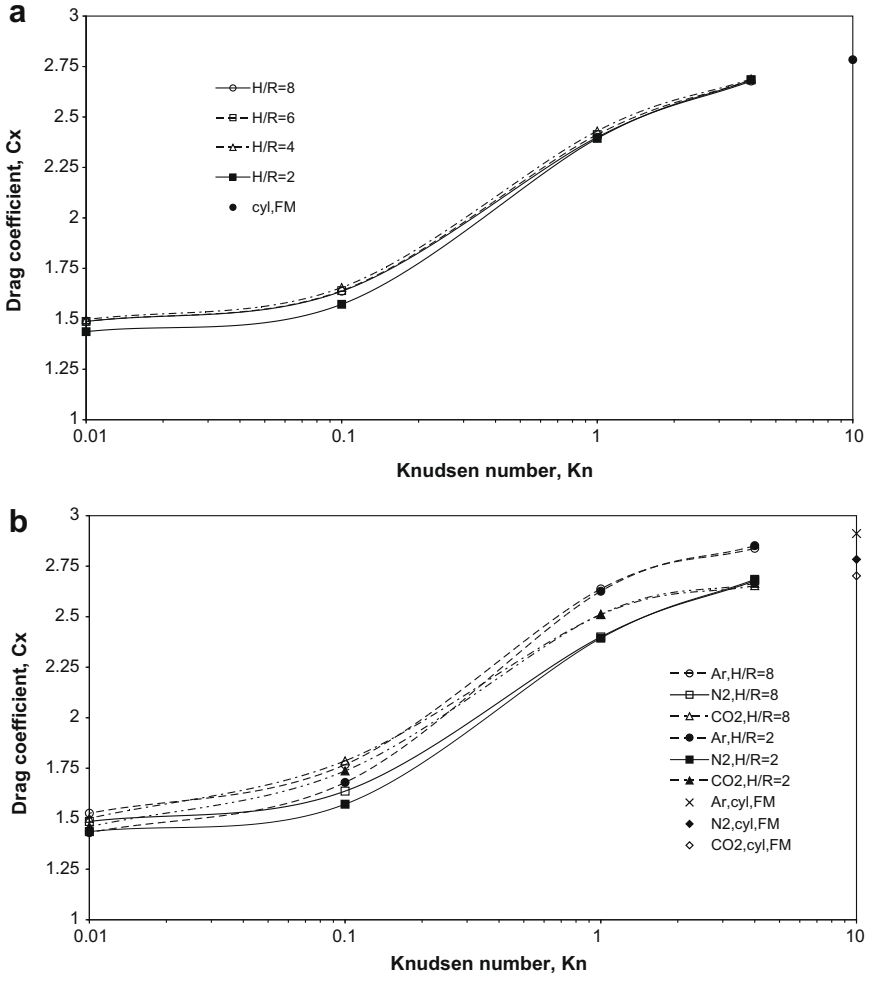

Fig. 9. Drag coefficient C_x of a torus vs. Knudsen number $Kn_{\infty,D}$ at $M_\infty = 10$ and various geometrical factors H/R: (a) in nitrogen flows and (b) in flows of argon, nitrogen, and carbon dioxide.

The DS2G program employed time averaging for steady flows [11]. About 200,000 samples have been studied in the considered cases. The computed results have been stored to the TECPLOT® files that have been further analyzed to study whether the DSMC numerical criteria [2] are met. Calculations were carried out on a personal computer with a Pentium® III 850-MHz processor. The computing time of each variant was estimated to be approximately 12–60 h.

4. Interference of two side-by-side plates

The flow pattern over two side-by-side plates is sensitive to the major geometrical similarity parameter, H/L. The influence of this factor on the stream structure has been studied for hypersonic flow of argon at $M_\infty = 10$ and $Kn_{\infty,L} = 0.024$. The flow pattern and shock-wave shapes are significantly different for large and small geometric ratios [21].

At $H/L = 1.0$, a strong oblique shock wave can be observed near the plate (see Fig. 3a). Two oblique shock waves interfere near the symmetry plane. The subsonic and supersonic areas (at $M \leqslant 2.5$) of the flow near the plates are symmetrical, which indicates that there is no lift force acting on the plates for the specified conditions. At $H/L = 0.5$, the flow near a plate becomes significantly asymmetrical, the disturbances interact in the vicinity of the symmetry plane, creating the Mach normal shock wave and a wide subsonic area, which occupies the whole "throat" area between

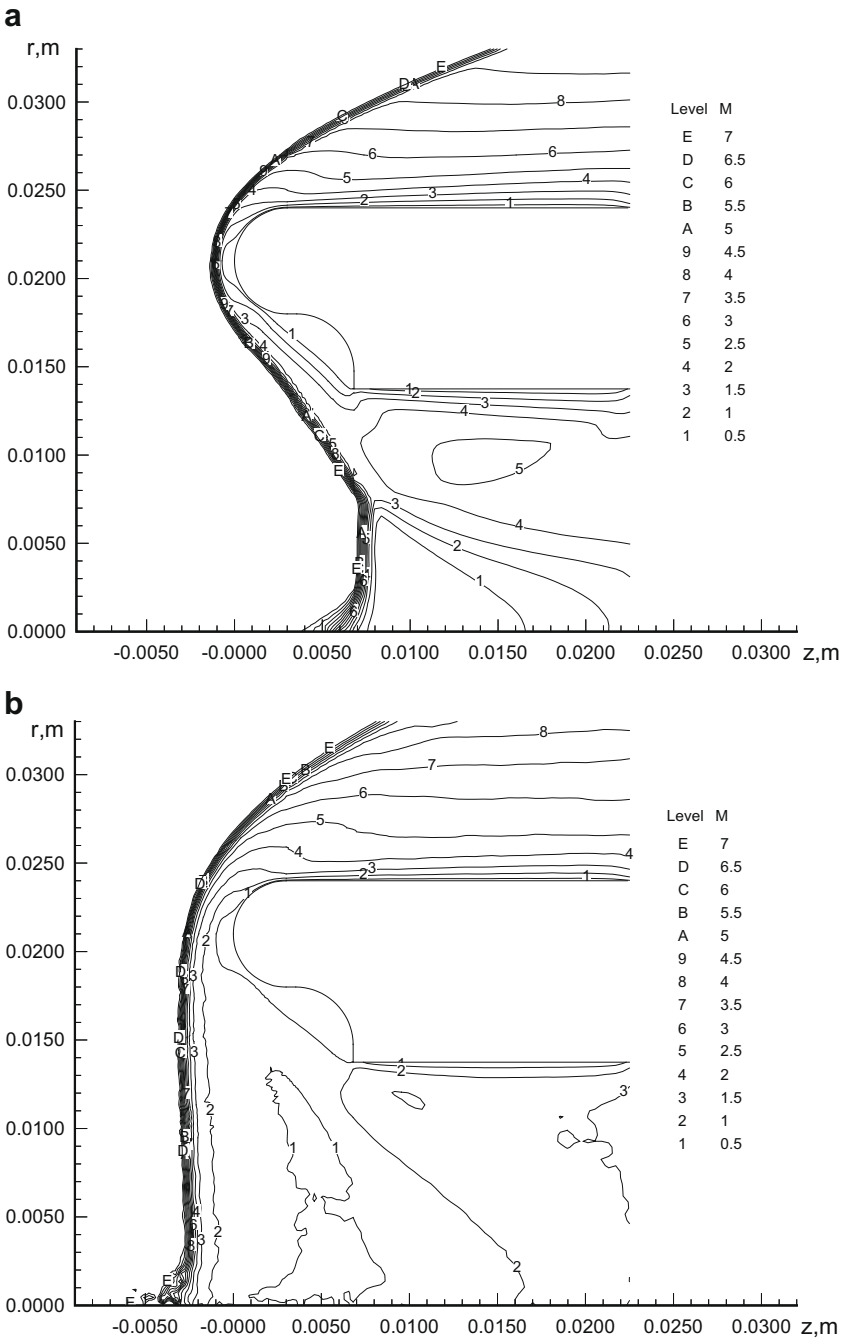

Fig. 10. Mach number contours in oxygen flow about a toroidal ballute model at $Kn_{\infty,D} = 0.005$: (a) dissociating oxygen flow and (b) perfect-gas oxygen flow.

two side-by-side plates (see Fig. 3b). The latter effect plays a fundamental role in the redistribution of pressure and skin friction along the plate surface (Fig. 4a and b, respectively). This phenomenon produces significant repulsive lift force. A non-monotonous dependency of lift and drag from values of the Knudsen number has been found for various geometric factors (see Fig. 5). The drag approaches the free-molecular limit [20] at $Kn_{\infty,L} > 2$.

The rarefaction effects on the lift force are significant at all considered values of the geometrical factor ($1.25 \geqslant H/L \geqslant 0.25$). At small factors, the repulsive lift force on side-by-side plates becomes significant with the lift-drag ratio of 1.6 in near-continuum flow regime and essentially reduces (up to 0.4) in the near-free-molecular flow.

5. Aerodynamics of two side-by-side cylinders

The flow pattern over two side-by-side cylinders is also sensitive to the major geometrical similarity parameter, H/R (see Fig. 6a and b). The influence of this parameter on the flow structure has been studied for hypersonic flow of argon at $M_\infty = 10$ and $Kn_{\infty,R} = 0.1$. At the small ratio parameters, $H/R \leqslant 2$, the front shock-wave shape becomes normal (see Fig. 6b), and front stagnation points (180°) relocate from the cylinder front zone towards the "throat" area (see Fig. 7a and b). This phenomenon [4,21] effects the drag, pressure and skin-friction distributions along a cylinder and produces significant repulsive lift force (see Fig. 8) with $C_y/C_x = 0.35$. The geometrical factor becomes insignificant on the

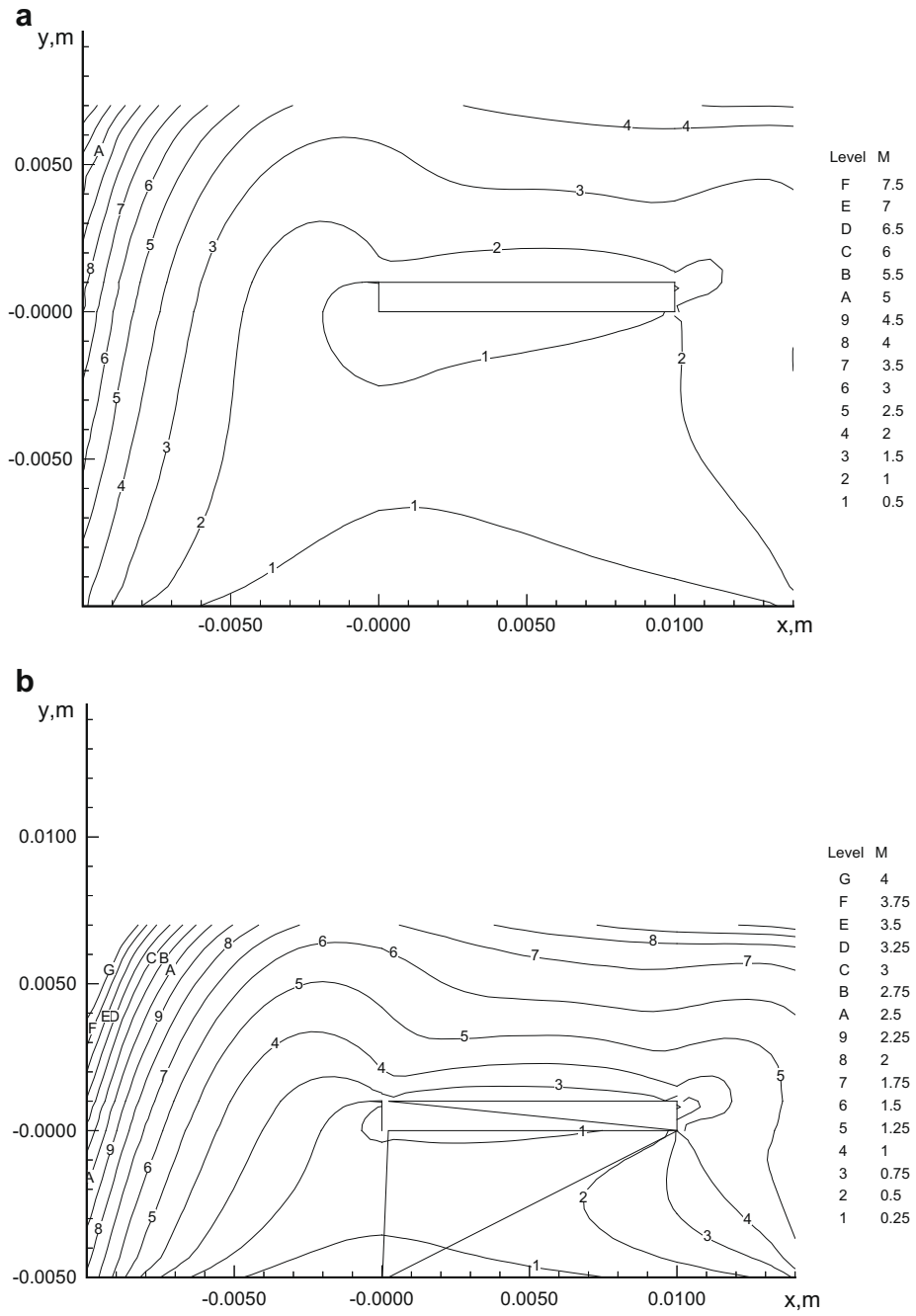

Fig. 11. Mach number contours in argon flow about a plate over a plane surface at $Kn_{\infty,L} = 0.07$ and various H/L-ratios: (a) $H = L$ and (b) $H = 0.5L$.

drag both under continuum flow regime conditions and in free-molecule flow at $H/R \geqslant 4$.

6. Flow over a toroidal ballute

Aerocapture with large inflatable decelerators known as toroidal ballutes [22] is currently viewed as the most promising technology for a number of NASA's future robotic missions to Venus, Saturn, Titan, and Neptune [23–26]. In the present study, the hypersonic rarefied-gas flows about a torus and ballute model have been studied. The flow pattern in argon was discussed in Ref. [7]. Several features of the flow are unique. For example, if the distance between the axis of symmetry and the torus disk center H is significantly larger the torus radius R, then the flow can be approximated by a stream between two side-by-side cylinders [12,19,21]. At $H = R$, the rarefied-gas flow has some features of a stream near a bluff disk [4,12]. In the first case, two conical shock waves would focus and interact in the vicinity of the symmetry axis generating the normal shock wave and the conical reflected waves. The stagnation points would be near the front points of the torus disks. In the second case, the front shock wave would be normal and the location of stagnation points would be difficult to predict. At $H > R$, the flow pattern and shock-wave shapes are very complex. As a result, simple approximation techniques would not be applied in torus aerothermodynamics.

In the present study, flows about a torus [21,28] and its aerodynamic characteristics have been investigated under the conditions of a hypersonic rarefied-gas stream of nitrogen, argon, dissociating oxygen, and carbon dioxide at $8R \geqslant H \geqslant 2R$ and the Knudsen number $Kn_{\infty,D}$ from 0.01 to 10.

The rarefaction factor, which can be characterized by the Knudsen number $Kn_{\infty,D}$, plays an important role in the flow structure [2,7] as well as in aerodynamics [4]. Under continuum flow conditions ($Kn_{\infty,D} = 0.01$), the flow structure has the same features as were discussed above. In transitional flow regime, at $Kn_{\infty,D} = 1$, the flow pattern is different [21,28]. The reflection waves have different shapes, because of the rarefaction effects in the conic and normal shock waves. At a small outer torus radius, $H/R = 2$, the skin-friction coefficient distribution along the torus surface becomes sensitive to the rarefaction parameter $Kn_{\infty,D}$ [28]. The locations of the front stagnation points are also changed at different Knudsen numbers.

The calculating results of the total drag coefficient are shown in Fig. 9. At any outer–inner radii ratio, the drag coefficient increases with increasing the Knudsen number. The geometrical factor becomes insignificant on the drag at $H/R \geqslant 6$ under continuum flow regime conditions (Fig. 9a), and at $H/R \geqslant 4$ in free-molecule flow regime. The influence of a ratio of the specific heats γ on drag of a torus is moderate (about 10%) for transition rarefied-flow regimes (Fig. 9b). The drag coefficient is more sensitive to the parameter γ in near-free-molecule flow regimes [20,28].

7. Aerodynamics of toroidal ballute models in dissociating and perfect gas flows

The hypersonic flows of oxygen near a toroidal ballute model [26,27] have been investigated numerically with the DSMC technique [2,11] under transitional rarefied conditions (Knudsen numbers $Kn_{\infty,D}$ from 0.005 to 1).

The effect of dissociation on chocking of ducted flows has been studied numerically for a ballute model with varying area ratio H/H^*. The present study confirms the hypothesis [27] that the flow of dissociating gas (oxygen) (Fig. 10a) is not choked at the "designed" toroid [27] with a throat radius $H^* = 0.014$ m, but the flow of perfect gas (Fig. 10b) is choked at the similar conditions [28]. The following parameters were used in calculations: $Kn_{\infty,D} = 0.005$, toros radius $R = 0.003$ m, upstream velocity $U_\infty = 5693$ m/s, static pressure $p_\infty = 1.28$ kPa, and temperature $T_\infty = 1415$ K.

8. Plate over a plane surface

In the case of a plate over a surface [21], the subsonic area between the plane surfaces becomes much wider than in the case of two side-by-side plates (see Fig. 11a and b). The detached shock wave interacts with the growing boundary layer above the surface. For $Kn_{\infty,L} = 0.071$ and $M_\infty = 10$, this effect results in a significant increase (20%) of the repulsive lift force at $2H/L \geqslant 1$ (see Fig. 12).

9. Cylinder over a plane surface

The argon flow about a cylinder located over a plane surface has been considered at $Kn_{\infty,L} = 0.1$ and $M_\infty = 10$. At a large distance between them, $H \geqslant 6R$, the interference of the shock waves does not change significantly the symmetrical flow near the cylinder (see Fig. 13a), and the repulsive lift force is negligible [21]. At the smaller ratio parameters, $H/R \leqslant 4$, the front shock-wave shape becomes normal (see Fig. 13b) and, as a result of interference between the shock wave and the growing boundary layer near the surface, the subsonic area about the cylinder becomes asymmetrical and much wider than in the case of two side-by-side cylinders. The latter effect results in a significant increase (more than 20%) of the repulsive lift force at $H/R \leqslant 4$.

10. Plate in the wake of a cylindrical wire

In the present analysis, the major regularities in hypersonic rarefied-gas flow about a plate ($L = 0.01$ m) with a thickness ratio $0.01 \leqslant t/L \leqslant 0.1$ located in the wake of a circular cylinder (10^{-4} m $\leqslant D \leqslant 10^{-3}$ m) have been studied under the conditions [13–17,21] of the strong interaction regime. The analysis of two-dimensional nitrogen flow is made using the DSMC technique [2,11] for rarefied-gas flow regimes at Knudsen number $Kn_{\infty,L} = 0.004$, Mach number $M_\infty = 15$, stagnation temperature $T_0 = 1100$ K, and wall temperature $T_w = 295$ K.

The influence of the geometrical factors of interference between a plate and a cylinder (i.e., the distance between the leading edge of a plate and a rear point of a cylinder, Δ, and the ratio of the cylinder diameter to the plate thickness, D/t) on flowfield characteris-

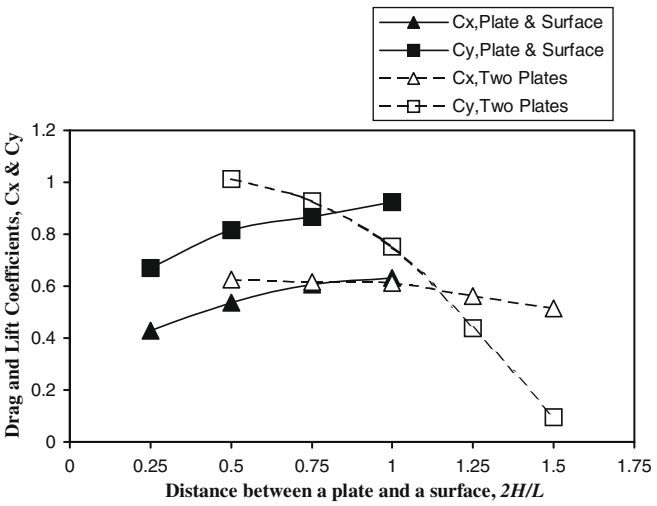

Fig. 12. Total drag and lift coefficients of a plate over a surface vs. coefficients of two side-by-side plates.

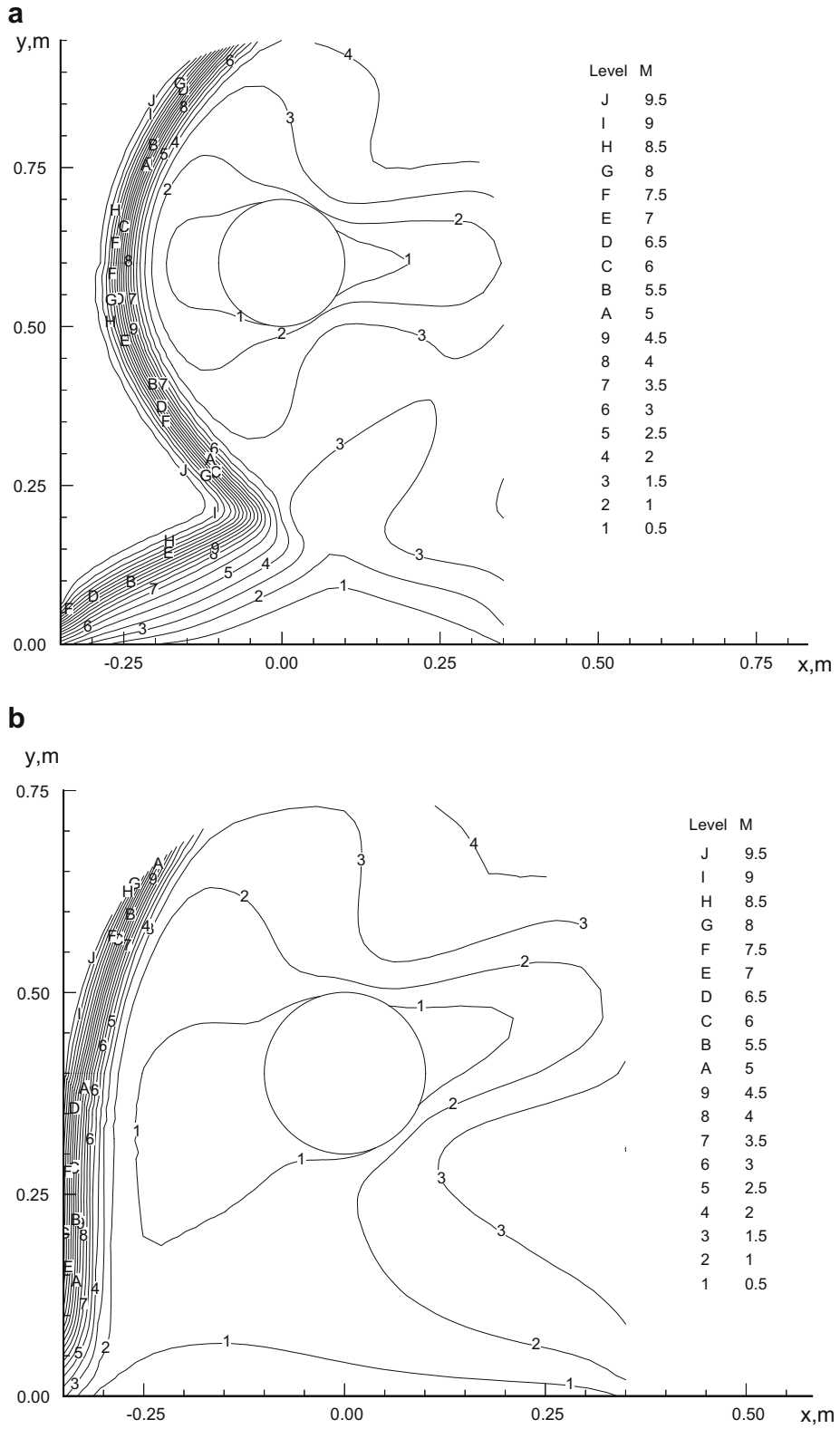

Fig. 13. Mach number contours in argon flow about a cylinder over a plate at $Kn_{\infty,R} = 0.1$ and various H/R-ratios: (a) $H = 6R$ and (b) $H = 4R$.

tics, skin-friction and pressure distributions along the surfaces of the bodies, and on the drag has been studied. The location of the external boundary with the upstream flow conditions varies from $2D$ to $5D$. The wake behind the cylinder interacts with the shock wave near the leading edge of a plate. This interaction results in increasing the size of subsonic zone [21] and in redistributing pressure and skin friction along the plate. The flow pattern is different for various D/t-ratios. The induced wake flow in the front area of the plate reduces the strength of the shock wave and results in reducing the plate drag up to 8.3% (see Fig. 14) and friction – up

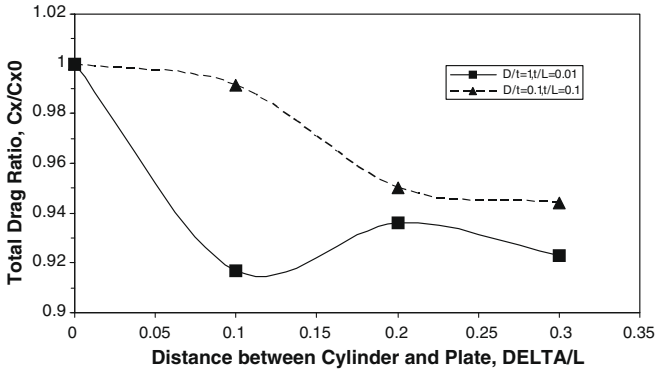

Fig. 14. Effect of the distance between cylinder and plate, Δ, on the total drag of the plate.

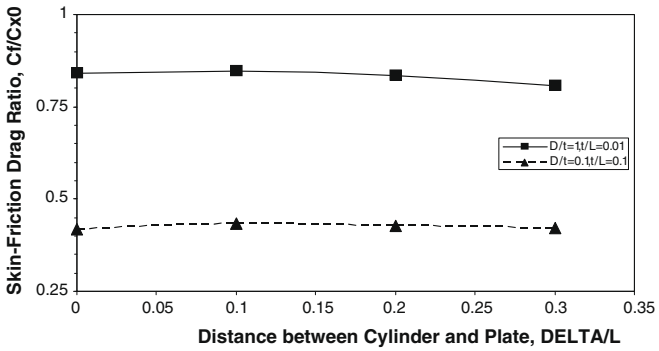

Fig. 15. Effect of the distance between cylinder and plate, Δ, on the skin-friction drag of the plate.

to 5% (see Fig. 15). The maximal reduction of the plate drag is observed at $D/t = 1$ and $\Delta/L = 0.1$. These findings are in the qualitative agreement with experimental data of Bisch [16].

11. Concluding remarks

The hypersonic rarefied-gas flows about two side-by-side plates and cylinders, a plate and cylinder over a plane surface, and a plate behind a cylinder in argon and nitrogen have been studied using the direct simulation Monte-Carlo technique. The flow pattern and shock-wave shapes are significantly different for small and large geometric ratios. At a value of the geometrical ratio parameter H/L of 0.5, the disturbances interact in the vicinity of the symmetry plane, creating a normal shock wave and a wide subsonic area, which occupies the whole "throat" area between the plates. This phenomenon affects the drag, pressure and skin-friction distributions along the plates, and produces significant repulsive lift force. A non-monotonic dependency of lift, drag and lift-drag ratio vs. Knudsen number has been found for different geometric factors. The rarefaction effects on the lift force are significant at all considered values of the geometric factor ($1.25 \geqslant H/L \geqslant 0.25$), and they are responsible for non-monotonic dependency of the lift force and lift-drag ratio with the maximum value of 1.7.

The similar effects have been found in the case of hypersonic argon flow about two side-by-side cylinders. At the small ratio parameters, $H/R \leqslant 3$, the front shock-wave shape becomes normal, a wide subsonic area occupies the whole "throat" area between the cylinders, and the front stagnation points relocate from the cylinder front zone to the throat area. This phenomenon affects the drag, pressure and skin-friction distributions along the cylinders, and produces significant repulsive lift force with the lift-drag ratio of 0.35.

Hypersonic flows about a toroidal balloon and its aerodynamic characteristics have been investigated in nitrogen, argon, dissociating oxygen, and carbon dioxide at $8R \geqslant H \geqslant 2R$ and the Knudsen number $Kn_{\infty,D}$ from 0.005 to 10. The effect of dissociation on chocking of ducted flows has been studied numerically for a ballute model with varying an aspect area ratio, H/H^*. The present study confirms the Lourel's hypothesis [27] that the flow of dissociating oxygen is not choked at the "designed" toroid with a throat radius $H^* = 0.014$ m, but the flow of perfect gas is choked at the similar conditions.

The subsonic area between the plate and a plane surface becomes much wider than in the case of two side-by-side plates. This effect results in the significant increase (more than 20%) in the repulsive lift force at $2H/L \geqslant 1$.

In the case of a blunt plate located in the wake of a cylindrical wire, the induced wake flow in front of the plate reduces the strength of the shock wave and results in reducing the plate drag up to 8.3%. The considered examples demonstrate the importance of studying the interference effects in applied hypersonic aerodynamics.

Acknowledgments

The author would like to express gratitude to Dr. G.A. Bird for the opportunity of using the DS2G computer program, Dr. J.N. Moss for valuable discussions of the DSMC technique, and to I. Lourel for providing experimental data received at the X2 expansion tube of the University of Queensland, Brisbane, Australia.

References

[1] Koppenwallner G, Legge H. Drag of bodies in rarefied hypersonic flow. In: Moss JN, Scott CD, editors. Thermophysical aspects of reentry flows. Progress in astronautics and aeronautics, vol. 103. New York (NY): AIAA; 1994. p. 44–59.
[2] Bird GA. Molecular gas dynamics and the direct simulation of gas flows. Oxford, England, UK: Oxford University Press; 1994. p. 340–77.
[3] Gusev VN, Erofeev AI, Klimova TV, Perepukhov VA, Riabov VV, Tolstykh AI. Theoretical and experimental studies of flow over bodies of simple shape by a hypersonic stream of rarefied gas. Trudy TsAGI 1977;1855:3–43 [in Russian].
[4] Riabov VV. Comparative analysis of hypersonic rarefied gas flows near simple-shape bodies. J Spacecraft Rockets 1998;35(4):424–33.
[5] Gorelov SL, Erofeev AI. Qualitative features of a rarefied gas flow about simple shape bodies. In: Belotserkovskii OM, Kogan MN, Kutateladze SS, Rebrov AK, editors. Rarefied gas dynamics. 13th International symposium proceedings, vol. 1. New York (NY): Plenum Press; 1985. p. 515–21.
[6] Lengrand JC, Allège J, Chpoun A, Raffin M. Rarefied hypersonic flow over a sharp flat plate: numerical and experimental results. In: Shizdal BD, Weaver DP, editors. Rarefied gas dynamics: space science and engineering. Progress in astronautics and aeronautics, vol. 160. New York (NY): AIAA; 1994. p. 276–84.
[7] Riabov VV. Numerical study of hypersonic rarefied-gas flows about a torus. J Spacecraft Rockets 1999;36(2):293–6.
[8] Coudeville H, Trepaud P, Brun EA. Drag measurements in slip and transition flow. In: de Leeuw JH, editor. Rarefied gas dynamics. Fourth international symposium proceedings, vol. 1. New York (NY): Academic Press; 1965. p. 444–66.
[9] Mavriplis C, Ahn JC, Goulard R. Heat transfer and flowfields in short microchannels using direct simulation Monte Carlo. J Thermophys Heat Transfer 1997;11(3):489–96.
[10] Oh CK, Oran ES, Sinkovits RS. Computations of high-speed, high Knudsen number microchannel flows. J Thermophys Heat Transfer 1997;11(3):497–505.
[11] Bird GA. The DS2G program user's guide, version 3.2. Killara, Australia: G.A.B. Consulting Pty; 1999. p. 1–56.
[12] Blevins RD. Applied fluid dynamics handbook. Malabar, FL: Krieger Publishing; 1992. p. 318–33.
[13] Hayes WD, Probstein RF. Hypersonic flow theory. New York (NY): Academic Press; 1959. p. 35–67.
[14] Oguchi H. The sharp-leading-edge problem in hypersonic flow. In: Talbot L, editor. Rarefied gas dynamics. Second international symposium proceedings. New York (NY): Academic Press; 1961. p. 501–24.
[15] Allègre J, Bisch C. Angle of attack and leading edge effects on the flow about a flat plate at Mach number 18. AIAA J 1968;6(5):848–52.
[16] Bisch C. Drag reduction of a sharp flat plate in a rarefied hypersonic flow. In: Potter JL, editor. Rarefied gas dynamics. 10th International symposium proceedings, vol. 1. Washington, DC: AIAA; 1976. p. 361–77.

[17] Yegorov IV, Yegorova MV, Ivanov DV, Riabov VV. Numerical study of hypersonic viscous flow about plates located behind a cylinder. AIAA Paper 97-2573. Washington, DC: AIAA; 1997. p. 1–10.
[18] Riabov VV. Aerodynamics of two side-by-side plates in hypersonic rarefied-gas flows. J Spacecraft Rockets 2002;39(6):910–6.
[19] Riabov VV. Interference between two side-by-side cylinders in hypersonic rarefied-gas flows. AIAA Paper 2002-3297. Washington, DC: AIAA; 2002. p. 1–9.
[20] Kogan MN. Rarefied gas dynamics. New York (NY): Plenum Press; 1969. p. 345–90.
[21] Riabov VV. Aerodynamics of two interfering simple-shape bodies in hypersonic rarefied-gas flows. In: Ketsdever AD, Muntz EP, editors. Rarefied gas dynamics. 23rd International symposium proceedings, vol. 663. Melville, NY: American Institute of Physics; 2003. p. 489–96.
[22] Hall JL, Le AK. Aerocapture trajectories for spacecraft with large, towed ballutes. AAS/AIAA Space Flight Mechanics Meeting, Paper AAS 01-235. Washington, DC: AIAA; 2001. p. 1–10.
[23] Gnoffo PA, Anderson BP. Computational analysis of towed ballute interactions. AIAA Paper 2002-2997. Washington, DC: AIAA; 2002. p. 1–9.
[24] Moss JN. DSMC simulations of ballute aerothermodynamics under hypersonic rarefied conditions. AIAA Paper 2005-4949. Washington, DC: AIAA; 2005. p. 1–15.
[25] McIntyre TJ, Lourel I, Eichman TN, Morgan RG, Jacobs PA, Bishop AI. Experimental expansion tube study of the flow over a toroidal ballute. J Spacecraft Rockets 2004;41(5):716–25.
[26] Lourel I., Eichmann TN, Isbister S, McIntyre TJ, Houwing AFP, Morgan RG. Experimental and numerical studies of flows about a toroidal ballute. In: Proceedings of the 23rd international symposium on shock waves, Paper 5038. Fort Worth, TX, July 22–27, 2001. p. 1–7.
[27] Lourel I, Morgan RG. The effect of dissociation on chocking of ducted flows. AIAA Paper 2002-2894. Washington, DC: AIAA; 2002. p. 1–11.
[28] Riabov VV. Numerical study of hypersonic rarefied-gas flows about a toroidal ballute. In: Ivanov MS, Rebrov AK, editors. Rarefied gas dynamics. 25th International symposium proceedings, vol. 1. Novosibirsk: Russian Academy of Sciences; 2007. p. 765–70.
[29] Riabov VV, Botin AV. Hypersonic hydrogen combustion in the thin viscous shock layer. J Thermophys Heat Transfer 1995;9(2):233–9.
[30] Ferziger J, Kaper HG. Mathematical theory of transport processes in gases. Amsterdam: North-Holland; 1972. p. 37–229.
[31] Riabov VV. Aerodynamic applications of underexpanded hypersonic viscous jets. J Aircraft 1995;32(3):471–9.
[32] Bird GA. Direct simulation of the Boltzmann equation. Phys Fluids 1970;13(11):2676–81.